

Spin thermopower in the overscreened Kondo model

This content has been downloaded from IOPscience. Please scroll down to see the full text.

2013 New J. Phys. 15 105023

(<http://iopscience.iop.org/1367-2630/15/10/105023>)

View [the table of contents for this issue](#), or go to the [journal homepage](#) for more

Download details:

This content was downloaded by: rokzitko

IP Address: 212.235.211.120

This content was downloaded on 23/10/2013 at 16:04

Please note that [terms and conditions apply](#).

Spin thermopower in the overscreened Kondo model

R Žitko^{1,2,4}, J Mravlje^{1,3}, A Ramšak^{1,2} and T Rejec^{1,2}

¹ J Stefan Institute, Jamova 39, SI-1000 Ljubljana, Slovenia

² Faculty for Mathematics and Physics, University of Ljubljana, Jadranska 19, SI-1000 Ljubljana, Slovenia

³ Collège de France, 11 Place Marcelin Berthelot, F-75005 Paris, France

E-mail: rok.zitko@ijs.si

New Journal of Physics **15** (2013) 105023 (15pp)

Received 5 July 2013

Published 23 October 2013

Online at <http://www.njp.org/>

doi:10.1088/1367-2630/15/10/105023

Abstract. Using the numerical renormalization group method, we study the spin thermopower in the two-channel spin-1/2 Kondo model. The non-Fermi liquid properties related to the overscreening of the impurity spin crucially affect the response of the system to the magnetic field and in consequence the spin-thermal transport. Although the magnetic field does not strongly polarize the impurity spin, we show that it nevertheless strongly affects the low-energy part of the spectral function. In turn, this leads to characteristic saturation of the spin Seebeck coefficient at the value of $0.388k_B/|e|$ at $T \sim T^*$, where $T^* \propto B^2/T_K$ is the scale of the crossover between the intermediate-temperature non-Fermi-liquid regime and the low-temperature Fermi-liquid regime. We show that measuring the spin thermopower at low magnetic fields would provide a sensitive test for distinguishing regular Fermi liquid, singular Fermi liquid and non-Fermi liquid behaviour in nanodevices.

⁴ Author to whom any correspondence should be addressed.



Content from this work may be used under the terms of the [Creative Commons Attribution 3.0 licence](https://creativecommons.org/licenses/by/3.0/). Any further distribution of this work must maintain attribution to the author(s) and the title of the work, journal citation and DOI.

Contents

1. Introduction	2
2. Models, spin thermopower and method	4
3. Spin Seebeck coefficient of the overscreened Kondo effect	6
4. Analysis of the asymptotic behaviour and the non-Fermi-liquid–regular Fermi-liquid crossover	7
5. Contrasting behaviour of spin thermopower in regular, singular and non-Fermi liquids	8
6. Conclusion	12
Acknowledgments	12
Appendix. Spin Seebeck coefficient in single-channel problems	13
References	13

1. Introduction

The Kondo effect is one of the most intensely studied and well-understood many-particle effects which occur due to strong interactions [1]. It may be adequately described by the Kondo model, a simple s – d exchange Hamiltonian for a point-like spin-1/2 impurity coupled to a continuum of conduction-band electrons through an antiferromagnetic exchange interaction. Due to strong confinement of electrons in nanostructures (such as semiconductor quantum dots [2], atoms and molecules [3], fullerenes [4], segments of carbon nanotubes [5], etc), the Kondo effect is fairly ubiquitous in various nanostructures exhibiting the Coulomb blockade phenomenon [6]. It manifests as enhanced conductivity in valleys with odd electron occupancy when the temperature is reduced below the characteristic Kondo temperature, T_K . Many experiments have confirmed the universal properties predicted for the Kondo effect and demonstrated that simple impurity models well describe most experimental features. At low temperatures, most such models behave as regular Fermi liquids (RFL) [7]: the low-energy excitations are conventional fermionic quasiparticles [8, 9] which have analytical scattering properties in the vicinity of the Fermi energy [10].

In recent years, experimental realizations of more exotic types of the Kondo effect have also been reported. The underscreened Kondo effect occurs when a spin-1 impurity is effectively coupled to a single conduction band [3, 11–13]. The impurity spin is only partially screened and there is residual impurity magnetization and residual impurity entropy [14–17]. The scattering amplitude of electrons near the Fermi energy is not analytical and the conventional Fermi-liquid picture breaks down [10, 17]. Such systems are classified as singular Fermi liquids (SFL) [10]. Experimentally, this type of behaviour is found in molecules with a spin center, which are stretched between two electrodes in mechanically controllable break junctions [3, 11]. In these systems, the spin would in principle be fully screened, but the Kondo temperature of the second screening stage is much below the experimental temperature.

Another unusual type of the Kondo effect, the overscreened Kondo effect, occurs when a spin-1/2 impurity is effectively coupled to two independent conduction bands. The impurity is overscreened and an unusual non-Fermi-liquid (NFL) ground state emerges [18–21]. The low-energy excitations are not Dirac-electron-like quasiparticles, but rather Majorana fermions [22].

Experimentally, such behaviour was observed in a setup where a small quantum dot (the impurity) was coupled to conduction leads (first conduction band) and a big quantum dot (second conduction band) [23]. By careful tuning of system parameters, it has been shown that the transport properties scale with temperature and gate voltage in accordance with the two-channel Kondo (2CK) model.

The characterization of nanodevices through transport properties provides information about the spectral function of the system. The low-temperature differential conductance is a measure of the spectral density at the Fermi level. As it is relatively easy to measure, it remains the most commonly used experimental probe. Additional information can be gathered by measuring other transport properties, such as the thermopower (Seebeck coefficient), which is a sensitive probe of the particle–hole asymmetry of the spectral function [24, 25]. In this work, we study a related property, the spin thermopower (spin Seebeck coefficient) [25, 26]. It is defined as the induced spin voltage across the device at zero spin current in the presence of a temperature gradient. The spin Seebeck coefficient S_s probes the particle–hole asymmetry of the spectral function in the presence of external magnetic field. Since the different kinds of the Kondo effect have very different response to an applied magnetic field, they can be clearly distinguished by different behaviour of S_s as a function of magnetic field B and the temperature T , as will become evident in the following.

The spin thermopower in the conventional Kondo model (single-channel $S = 1/2$ model, which is a RFL) has been studied in [26]. Related results for the charge thermopower in the model with attractive interaction have been reported in [27]. For $T \lesssim T_K$, the spin thermopower as a function of B peaks at $B \sim T_K$ (B is measured in the units of the Zeeman energy $g\mu_B B$, while the temperature is measured in the units of energy $k_B T$). For $B \lesssim T_K$, the spin thermopower as a function of T peaks at $T \sim 0.3T_K$. Finally, for $B, T \gtrsim T_K$, the spin thermopower peaks at $B \sim 3T$. These features can be well understood within a simple model for the Kondo peak splitting in applied magnetic field, taking into account thermal broadening effects.

The spin thermopower in the underscreened Kondo model (single-channel $S = 1$ model, which is SFL [16, 17]) has been studied in [25]. Due to the decoupled residual impurity moment, even a tiny magnetic field strongly polarizes the impurity and splits the Kondo peak. The main difference between the $S = 1/2$ and 1 models is thus in the $B \lesssim T_K$ regime, where the maximum in the spin thermopower as a function of T is now found for $T \sim 0.2B$, rather than at constant $T \sim 0.3T_K$; the amplitude of the maximum is comparable in both the cases, being somewhat smaller in the underscreened case in a wide parameter range.

The spin thermopower in the overscreened Kondo model (two-channel $S = 1/2$ Kondo model, which is a true NFL system) is the subject of this work. The magnetic field is a relevant perturbation which drives the system away from the NFL fixed point, which governs the behaviour of the system in the temperature range $T^* \ll T \ll T_K$, to the stable low-temperature RFL fixed point at $T \ll T^*$. We will show that the 2CK model exhibits very peculiar low-field behaviour of the spin thermopower, which has a maximum at the crossover scale $T^* \propto B^2/T_K$ with a height which saturates at small B (unlike in the fully screened and underscreened cases, where the height goes to zero). The saturated value at the maximum is $0.388k_B/|e| \approx 34\mu\text{V K}^{-1}$. We will compare the very interesting contrasting behaviour of the underscreened and overscreened models: while in the underscreened model, a small magnetic field that strongly polarizes the impurity spin affects mainly the high-energy part of the spectral function, in the overscreened model the polarization effect is small but it strongly affects especially the

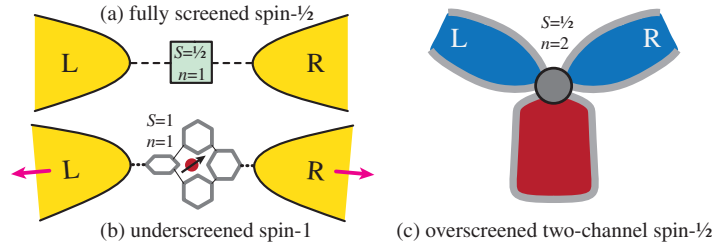


Figure 1. Schematic representation of the three nanodevices which can be described using the spin- S n -channel Kondo model. (a) Semiconductor quantum dot. (b) Spin-1 molecule [3, 11]. (c) Quantum dot coupled to a large quantum dot [23].

low-energy part of the spectral function, thus leading to a large spin-thermal response at T^* for any non-vanishing field.

2. Models, spin thermopower and method

The physical systems discussed in this work are schematically represented in figure 1. The nanodevice is coupled to two contacts kept at different temperatures. The electrons in these two contacts form one screening channel. In addition, in the 2CK case, the role of the second screening channel is played by the electrons in the additional large quantum dot. The electrons in this dot are electrostatically confined by the large Coulomb repulsion in order to eliminate processes in which an electron would tunnel from the large quantum dot to the contacts; such processes would destroy the two-channel physics (i.e. they correspond to an additional relevant operator which drives the system away from the NFL fixed point).

At temperatures low enough, such nanosystems can all be modeled using some variant of the Kondo impurity model, where the impurity degrees of freedom are described using a quantum mechanical spin operator \mathbf{S} which is locally coupled with the spin density of the conduction band electrons. The corresponding Hamiltonian is thus

$$H = \sum_{\mathbf{k}, \sigma, i} \epsilon_{\mathbf{k}} c_{\mathbf{k}, \sigma, i}^{\dagger} c_{\mathbf{k}, \sigma, i} + \sum_{\alpha} J s_{\alpha} \cdot \mathbf{S} + \mathbf{B} \cdot \mathbf{S}, \quad (1)$$

where $c_{\mathbf{k}, \sigma, i}^{\dagger}$ are creation operators for the itinerant electrons in channel i with momentum \mathbf{k} , spin σ and energy $\epsilon_{\mathbf{k}}$. The spin density of the band i can be expressed as

$$\mathbf{s}_i = \frac{1}{N} \sum_{\mathbf{k}, \mathbf{k}'} \sum_{\alpha \beta} c_{\mathbf{k}, \alpha, i}^{\dagger} \left(\frac{1}{2} \boldsymbol{\sigma}_{\alpha \beta} \right) c_{\mathbf{k}', \beta, i} = \sum_{\alpha \beta} f_{0, \alpha, i}^{\dagger} \left(\frac{1}{2} \boldsymbol{\sigma}_{\alpha \beta} \right) f_{0, \beta, i}. \quad (2)$$

Here $f_{0, \sigma, i}^{\dagger} = (1/\sqrt{N}) \sum_{\mathbf{k}} c_{\mathbf{k}, \sigma, i}^{\dagger}$ is the combination of states which couples to the impurity, while $\boldsymbol{\sigma} = \{\sigma^x, \sigma^y, \sigma^z\}$ is a vector of Pauli matrices. The index i ranges over the number of channels n (one or two). Depending on the value of the impurity spin S and the number of channels n , the impurity spin will be either fully screened ($n = 2S$), underscreened ($n < 2S$) or overscreened ($n > 2S$) [18, 28–32]. We fix the Kondo exchange coupling J to a constant value $J/D = 0.2$. Here D is the half-width of the conduction band which is assumed to have a flat density of states $\rho = 1/2D$. The half-bandwidth is also used as the energy unit, $D = 1$.

The Kondo temperature is the same (up to non-exponential prefactors) in all the three models, $T_K \propto \exp(-1/\rho J)$. Numerically, we find

$$T_{K,W} = 1.1 \times 10^{-5}, \quad (3)$$

where $T_{K,W}$ is the Kondo temperature as defined by Wilson through the impurity magnetic susceptibility, $T_{K,W} \chi_{\text{imp}}(T_{K,W}) = 0.07$ [33, 34]. The magnetic field is measured in units of the Zeeman energy (i.e. we absorb the factor $g\mu_B$ into B).

In this work, we focus on the spin Seebeck coefficient S_s , defined as [26]

$$S_s = -\left. \frac{V_s}{\Delta T} \right|_{I_s=0}.$$

The spin thermopower is the ability of the device to convert the temperature difference ΔT to spin voltage V_s , assuming no spin current I_s flows through the impurity. In units of $k_B/|e|$, to be used in what follows, the spin Seebeck coefficient

$$S_s = \frac{2}{T} \frac{\mathcal{I}_1}{\mathcal{I}_0} \quad (4)$$

is determined by computing the transport integrals

$$\mathcal{I}_{n\sigma} = \int d\omega \omega^n [-f'(\omega)] \mathcal{T}_\sigma(\omega), \quad (5)$$

where $f(\omega)$ is the Fermi–Dirac function at temperature T . At the particle–hole symmetric point (the case considered in this work), one has $\mathcal{I}_{0\uparrow} = \mathcal{I}_{0\downarrow} \equiv \mathcal{I}_0$ and $\mathcal{I}_{1\uparrow} = -\mathcal{I}_{1\downarrow} \equiv \mathcal{I}_1$. From the definition it is manifest that the spin thermopower probes the difference in the particle–hole asymmetry of the two spin species.

The quantity \mathcal{T}_σ in equation (5) is the transmission function of electrons with spin σ in the first channel (i.e. the channel which corresponds to the source and drain leads). It is proportional to the imaginary part of the T matrix for the Kondo model, defined as $G = G_0 + G_0 T G_0$, where G is the interacting Green’s function for electrons, while G_0 is the non-interacting one. For a given model, it may be computed using the equation of motion approach. One finds $\mathcal{T}_\sigma = \langle\langle O_\sigma; O_\sigma^\dagger \rangle\rangle$, where O_σ is defined as the commutator between the annihilation operator on the first site of the Wilson chain (which is the same as the combination of conduction-band states which couples to the impurity, $f_{0,\sigma,1}$) and the Kondo coupling term, $O_\sigma = [H_{K,1}, f_{0,\sigma,1}]$, where $H_{K,1} = J\mathbf{s}_1 \cdot \mathbf{S}$. The result is a composite fermion operator [35, 36]

$$O_\alpha = \left(\frac{1}{2} \sum_\beta \sigma_{\alpha\beta} f_{0,\beta,1} \right) \cdot \mathbf{S}. \quad (6)$$

The transport integrals have been computed using the numerical renormalization group (NRG) method [33, 34, 37], using the approach described in [26]: the Lehmann representation of the spectral function is integrated over and the transport integrals $\mathcal{I}_{n\sigma}$ are computed for all temperatures in a single NRG sweep. It has been shown that for the RFL case this leads to only a very small deviation (few per cent at most) from the results of the more accurate full-density-matrix (FDM NRG) approach [38], and we have now verified that this is the case also for the SFL in magnetic field despite the strong magnetic polarizability of this model.

We conclude this section by a remark about the role of the second quantum dot as regards the particle and heat flow. We have assumed that the voltage and the temperature in the leads are

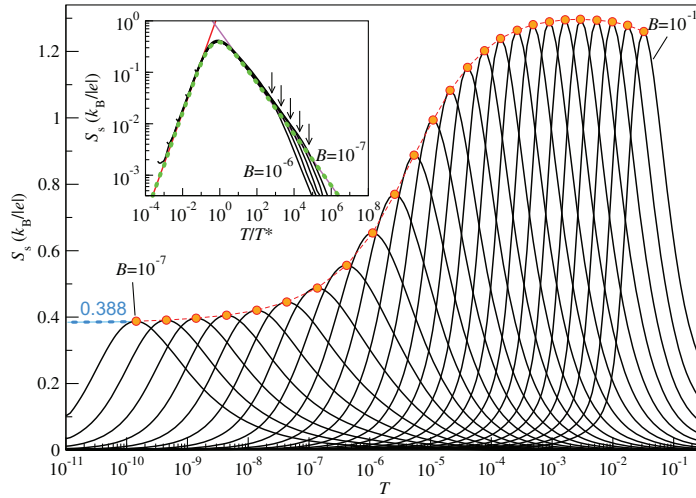


Figure 2. Spin Seebeck coefficient for the two-channel Kondo model. The magnetic field ranges from $B = 10^{-7}$ to 10^{-1} in steps of factor $10^{1/4}$. The colored dots indicate the positions of the peaks in the spin Seebeck coefficient for different values of B ; the positions, T_{\max} , and the corresponding values of the coefficient, $S_s(T_{\max})$, are plotted in figure 3 as a function of B . The inset shows how, for temperatures below the Kondo temperature (indicated by arrows), the curves for different fields from $B = 10^{-7}$ to 10^{-6} collapse into a universal curve given by equation (7) and shown with green dotted line. The low temperature, $T \ll T^*$, asymptote of equation (9) is shown as red line. The intermediate temperature, $T^* \ll T \ll T_K$, asymptote of equation (10) is shown as violet line.

symmetrically shifted with respect to the equilibrium value. For this reason, neither charge nor spin current flow to the large quantum dot. The large dot thus only plays the role of an additional screening channel.

3. Spin Seebeck coefficient of the overscreened Kondo effect

The main result of this work is shown in figure 2. We plot the spin Seebeck coefficient of the 2CK model for a range of applied external magnetic fields B as a function of T .

For any B , the spin thermopower curve has a single peak. For $B \ll T_K$, the peak occurs at the NFL–RFL crossover scale $T^* \propto B^2/T_K$. The B^2 scaling is a characteristic feature of the model and is not expected to be observed in single-channel models. In this regime, $S_s(T)$ at the point of its maximum saturates at a value that is determined using analytical arguments in the following section. (A somewhat related saturation of the charge Seebeck coefficient has been noted in a different proposed physical realization of the 2CK model [39]. In that case, the symmetry breaking operator was the channel asymmetry, $J_1 \neq J_2$.) The behaviour is universal and we find that the curves, when plotted as a function of T/T^* , fully overlap at low temperatures; see the inset in figure 2.

For $B \gg T_K$, the spin thermopower peaks on the temperature scale of B . Such asymptotic behaviour is expected for any impurity model where the local degrees of freedom are described by a spin operator. The reason is that for large B , there will be a threshold for inelastic spin

excitations given by the Zeeman energy. The spectral lineshapes, however, are expected to be model-dependent. (The small drop in the maximum of $S_s(T)$ at the largest values of B in figure 2 is due to finite-bandwidth effects.)

4. Analysis of the asymptotic behaviour and the non-Fermi-liquid–regular Fermi-liquid crossover

The NFL state of the 2CK model is destabilized by a perturbation due to an external magnetic field acting on the impurity, forcing the system towards a RFL ground state. In [40] the authors exploited a connection to an exactly solvable classical boundary Ising model to obtain the exact finite-temperature transmission function,

$$\mathcal{T}_\sigma(\omega, T) = \frac{1}{2} + \sigma \frac{1}{\sqrt{8\pi^3}} \int_{-\infty}^{\infty} dx \frac{\cos \frac{x\omega}{\pi T}}{\tanh \frac{\omega}{2T} \sinh x} \\ \times \text{Re} \left\{ \sqrt{\frac{T^*}{T}} \frac{\Gamma\left(\frac{1}{2} + \frac{1}{2\pi} \frac{T^*}{T}\right)}{\Gamma\left(1 + \frac{1}{2\pi} \frac{T^*}{T}\right)} {}_2F_1\left(\frac{1}{2}, \frac{1}{2}, 1 + \frac{1}{2\pi} \frac{T^*}{T}, \frac{1 - \coth x}{2}\right) \right\},$$

describing the crossover from low temperature, $T \ll T^*$, FL to intermediate temperature, $T^* \ll T \ll T_K$, NFL regime. Here Γ is the Gamma function and ${}_2F_1$ is the hypergeometric function. The crossover temperature scale,

$$T^* = c_B^2 \frac{B^2}{T_K},$$

is proportional to the square of the magnetic field, which should be small enough, $B \ll T_K$, to ensure that the crossover temperature is well separated from the Kondo temperature. $c_B = \mathcal{O}(1)$ is a fitting parameter; in our case $c_B = 0.436$. This theory applies exactly in the $B \ll T_K$ limit. We find that for the range of B considered in this work, the transmission function has a multiplicative field-dependent prefactor, which, however, largely cancels out when $S_s(T)$ is computed as a ratio of two transport integrals; thus the universal scaling for $S_s(T)$ applies well for $B/T_K \lesssim 10^{-1}$.

To evaluate the spin Seebeck coefficient, the integrals over ω in equations (3) and (4) can be calculated exactly. The spin Seebeck coefficient,

$$S_s = \frac{\sqrt{\pi}}{2\sqrt{2}} \int_{-\infty}^{\infty} dx \frac{1}{\cosh^2 \frac{x}{2} \sinh x} \text{Re} \left\{ \sqrt{\frac{T^*}{T}} \frac{\Gamma\left(\frac{1}{2} + \frac{1}{2\pi} \frac{T^*}{T}\right)}{\Gamma\left(1 + \frac{1}{2\pi} \frac{T^*}{T}\right)} {}_2F_1\left(\frac{1}{2}, \frac{1}{2}, 1 + \frac{1}{2\pi} \frac{T^*}{T}, \frac{1 - \coth x}{2}\right) \right\}, \quad (7)$$

is a universal function of rescaled temperature T/T^* . The inset to figure 1 shows how the NRG curves corresponding to different magnetic fields $B \ll T_K$ collapse into a universal curve at temperatures well below T_K . In this regime, the spin Seebeck coefficient reaches its maximum value of $S_s(T_{\max}) = 0.388$, independent of the field, at $T_{\max} = 0.829T^*$. We were unable to find a closed-form expression for $S_s(T_{\max})$, but it can be computed numerically as the maximum value of the expression in equation (7).

At low temperatures, $T \ll T^*$, the transmission function is well approximated by its zero temperature form. For $\omega \ll T^*$ the transmission function deviates from its $\omega = 0$ value,

$\mathcal{T}_\sigma(0, 0) = \frac{1}{2}$, in a linear fashion

$$\mathcal{T}_\sigma(\omega, 0) \stackrel{\omega \ll T^*}{\approx} \frac{1}{2} + \frac{\sigma}{8} \frac{\omega}{T^*}. \quad (8)$$

The deviation $|\mathcal{T}_\sigma(\omega, 0) - \frac{1}{2}|$ reaches its maximal value of 0.13 at $\omega \approx 4T^*$ and drops to zero as

$$\mathcal{T}_\sigma(\omega, 0) \stackrel{\omega \gg T^*}{\approx} \frac{1}{2} + \frac{\sigma}{2\sqrt{2\pi}} \frac{\ln \omega}{\sqrt{\omega}}$$

in the high frequency limit. The low-temperature spin Seebeck coefficient, probing the low-frequency part of the transmission function, equation (8),

$$S_s \stackrel{T \ll T^*}{\approx} \frac{2\pi^2}{3} T \left. \frac{\partial \ln \mathcal{T}_\uparrow(\omega, 0)}{\partial \omega} \right|_{\omega=0} = \frac{\pi^2}{6} \frac{T}{T^*} \quad (9)$$

exhibits a typical Fermi liquid linear dependence on temperature.

At higher temperatures, $T^* \ll T \ll T_K$, the transmission function takes a simpler form

$$\mathcal{T}_\sigma(\omega, T) = \frac{1}{2} + \sigma \sqrt{\frac{T^*}{T}} \frac{1}{\sqrt{2\pi^4}} \int_{-\infty}^{\infty} dx \frac{\cos \frac{x\omega}{\pi T}}{\tanh \frac{\omega}{2T} \sinh x} \operatorname{Re} \left\{ K \left(\frac{1 - \coth x}{2} \right) \right\},$$

where K is the complete elliptic integral of the first kind. It can be cast in a scaling form

$$\frac{\mathcal{T}_\sigma(\omega, T) - \frac{1}{2}}{\sqrt{\frac{T^*}{T}}} = \sigma \mathcal{F} \left(\frac{\omega}{T} \right),$$

where the scaling function \mathcal{F} is linear in frequency for $\omega \ll T$,

$$\mathcal{F}(u) \stackrel{u \ll 1}{\approx} 0.082u,$$

reaches a maximum value of 0.15 at $\omega \approx 5T$ and drops to zero as

$$\mathcal{F}(u) \stackrel{u \gg 1}{\approx} \frac{1}{2\sqrt{2\pi}} \frac{\ln u}{\sqrt{u}}$$

in the high-frequency limit. Such a scaling causes the spin Seebeck coefficient to exhibit an anomalous NFL dependence on temperature

$$S_s \stackrel{T \gg T^*}{\approx} \frac{4\sqrt{2}}{9} \sqrt{\frac{T^*}{T}}. \quad (10)$$

To sum it up, the spin Seebeck coefficient of the 2CK model at low B is characterized by an asymmetric peak of a universal form with a maximum value of about 0.4 at the crossover temperature T^* between RFL and NFL regimes. The low-temperature asymptote is proportional to T/T^* , while the high-temperature one is proportional to $\sqrt{T^*/T}$.

5. Contrasting behaviour of spin thermopower in regular, singular and non-Fermi liquids

In figure 3, we compare the main characteristics of the spin thermopower in the three models considered. As a function of the applied magnetic field we plot the following quantities: the temperature T_{\max} of the maximum, of the spin Seebeck coefficient $S_s(T)$, the value $S_s(T_{\max})$ of the spin Seebeck coefficient at this maximum, and the impurity magnetic moment

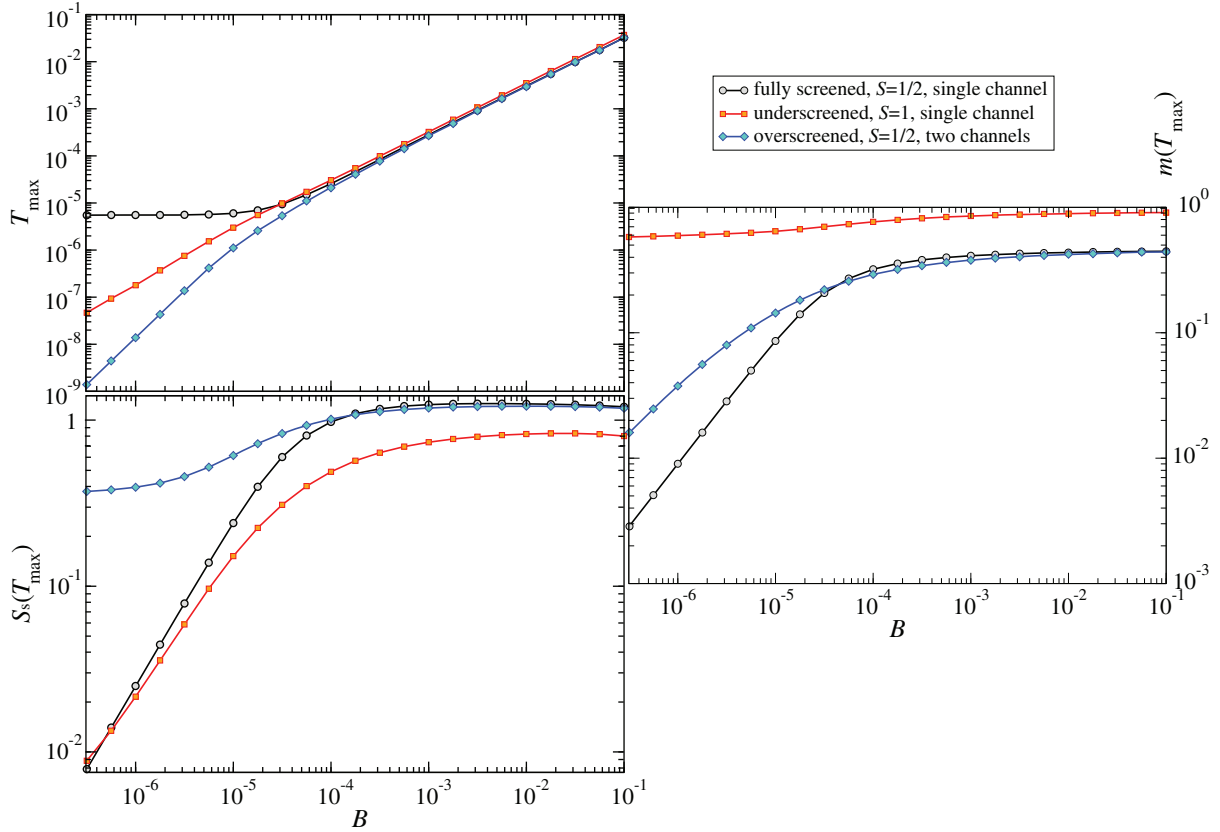


Figure 3. Top left: position of the peak of the spin Seebeck coefficient as a function of T for various values of the magnetic field B . Bottom left: value of the spin Seebeck coefficient at its peak. Right: the impurity spin polarization as a function of the magnetic field B at the temperature of the peak in the spin Seebeck coefficient.

$m(T_{\max}) = \langle S_z \rangle$ at the maximum of S_s . The first two quantities have been extracted from the results shown in figures 2 and A.1.

We first note that the high-field behaviour is rather similar in all the three models, as has been already suggested in section 3. We find that the temperature of the maximum is almost the same in all the three cases and given approximately by $T_{\max} \approx 0.3B$. The value of spin Seebeck coefficient at this maximum depends only on the impurity spin, not on the number of channels, and it saturates for high magnetic fields: for $S = 1/2$ we find $S_s(T_{\max}) \approx 1.32$, while for $S = 1$ we obtain a *smaller* value $S_s(T_{\max}) \approx 0.9$. The magnetizations at the maximum are also spin dependent: for $S = 1/2$ we find $m(T_{\max}) \approx 0.45$, while for $S = 1$ it is twice as large, $m(T_{\max}) \approx 0.9$.

A crude way to understand the high-field asymptotic behaviour is to postulate the following rough approximation for the transmission function in the large- B limit:

$$\mathcal{T}_\sigma(\omega) \propto 1 + cm\theta(\sigma\omega - B), \quad (11)$$

i.e. a piecewise constant function with a jump at $\omega = \sigma B$ by a value proportional to the magnetization with c a constant of order 1. The increase in scattering is due to the opening of the inelastic scattering channel due to spin-flips, which is possible for energies above the

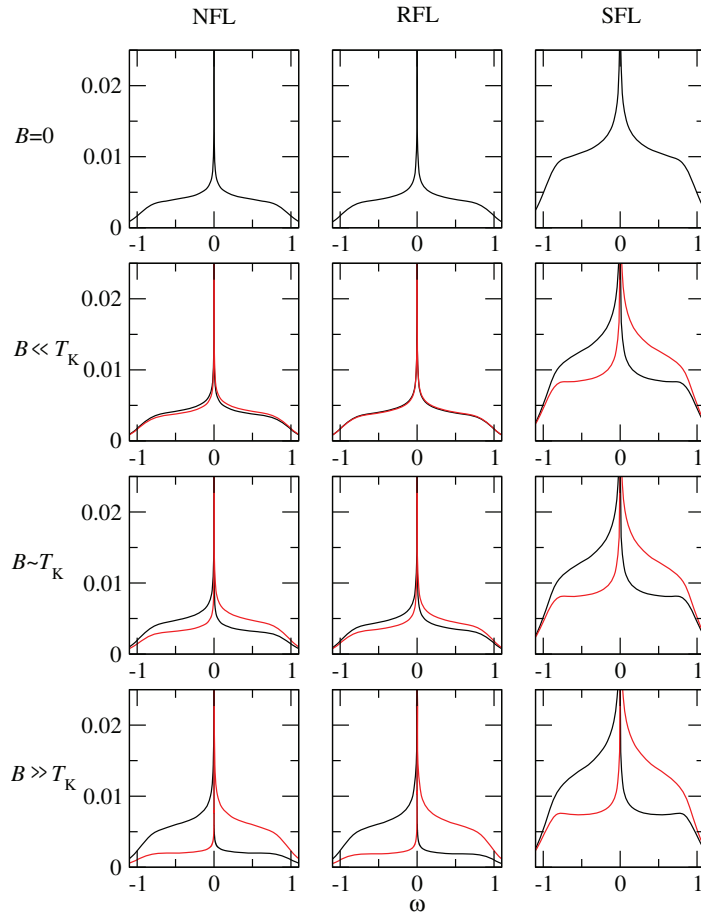


Figure 4. $T = 0$ spectra of the three models for a range of magnetic fields. The magnetic fields are $B = 10^{-6} \ll T_K$, $10^{-5} \sim T_K$ and $10^{-4} \gg T_K$. Red curves: spin up, $\sigma = \uparrow$, black curves: spin down, $\sigma = \downarrow$.

Zeeman energy. This form is suggested by the more accurate renormalization group theory [36]. We find that the spin Seebeck coefficient obtained using equation (11) has a peak at $T = 2.3B$ with a height of 0.89 (for $c = 1$ and taking the value of m from NRG). Considering the extreme crudeness of the model, the result is a fair approximation for the true values.

For all the three models, the crossover to the low-field behaviour occurs on the same scale of the Kondo temperature. The low-field asymptotic behaviour, however, is markedly different in the three models. In the RFL case, the maximum occurs at the constant temperature of $T \sim 0.3T_K$ [26]. This is because the impurity spectral function is not significantly affected by magnetic fields lower than T_K ; there is only a rigid shift of the two spin-projected components of the spectral function. The linear reduction of $S_s(T_{\max})$ is also well accounted for by simple Fermi liquid arguments [26]. RFLs exhibit Pauli paramagnetism with T_K playing the role of the Fermi temperature, thus the magnetization of this model at low temperatures is given by B/T_K .

In the SFL, the spin Seebeck coefficient peaks at a temperature on the scale where the system crosses over from the SFL regime at intermediate temperatures to the asymptotic RFL behaviour at low temperatures [10]. The crossover temperature, defined from the

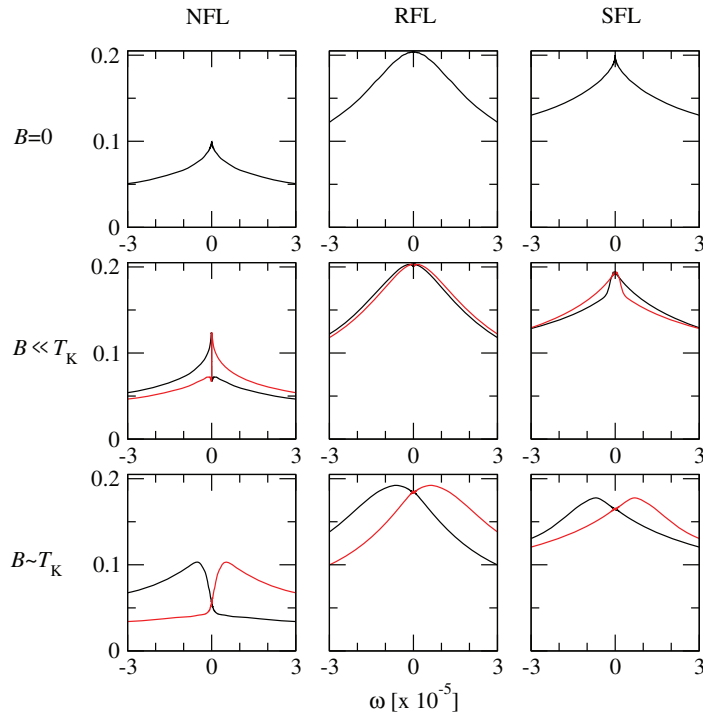


Figure 5. $T = 0$ spectra of the three models for a range of magnetic fields: close-up of the low-frequency region.

thermodynamic properties as the temperature where the impurity entropy decreases to one half of its value at the SFL fixed point, is found to be $T_{\text{td}} = 0.32B$, with no logarithmic correction. The position of the peak in S_s , T_{max} , appears to have logarithmic corrections compared to T_{td} . The maximum spin Seebeck coefficient $S_s(T_{\text{max}})$ decreases to zero as a linear function, but again with logarithmic corrections.

For completeness we also plot the impurity spin magnetization for the three models in the right panel of figure 3. We emphasize that strong spin polarization does not necessarily imply a large spin Seebeck coefficient. In fact, the underscreened model—with by far the largest polarization—has the smallest spin Seebeck coefficient in a wide interval of magnetic fields (in fact, only for $B < 10^{-2}T_K$ is its spin Seebeck coefficient somewhat larger than that of the fully screened model).

To better understand the value of the spin Seebeck coefficient we study the impurity spectral functions (figure 4). At $B = 0$, the overall aspect of the spectral functions is the same: they all have a Kondo resonance with a width proportional to T_K . The main differences are better visible in the close-up to the peak region, (figure 5). The resonance shape is analytical only in the RFL case. The approach to the asymptotic value in the SFL is logarithmic [17], while in the 2CK effect it has a square root non-analyticity [41, 42]. Note also that the $\omega = 0$ value of the spectral function is twice as big in RFL and SFL as compared to the NFL case [42]. For small fields, $B \ll T_K$; the effect on the overall spectral function is the most significant in the SFL case where a strong spin polarization clearly manifests on all frequency scales (see figure 4). Figure 5, however, reveals that in the NFL case the relative change of the spectral function *at low frequencies* is very significant. The spin-up spectral function is much higher

for $\omega > 0$ compared to $\omega < 0$ (by almost a factor of 2), and it peaks on the frequency scale of $T^* \propto B^2/T_K$. The peak height even exceeds the height of the zero-field spectral function at $\omega = 0$. This low-frequency polarization effect is much stronger compared to that for (singular and regular) Fermi liquid systems. This explains the large spin Seebeck coefficient in the NFL case.

6. Conclusion

We have analyzed the spin thermopower of the two-channel Kondo model, which is a paradigmatic case of an impurity model with non-Fermi-liquid properties at low-energy scales. We have shown that the crossover to the Fermi-liquid ground state generated by applied magnetic field $B < T_K$ leads to a pronounced peak in the spin Seebeck coefficient as a function of the temperature. The peak position correspond to the crossover scale $T^* \propto B^2/T_K$, while its height saturates at a sizeable value of $0.388k_B/|e|$. This is to be opposed to the single-channel Kondo models with $S = 1/2$ (RFL) and $S = 1$ (SFL), where for $B < T_K$ the peak height decreases at low B . These differences arise due to characteristically distinct ways in which the magnetic field affects the spectral function in different cases. In the 2CK model, the spectral function becomes strongly spin-dependent on the lowest energy scales, in stark contrast to the strongly spin polarizable underscreened $S = 1$ model, where the spin dependence is large on higher-energy scales, but is less pronounced in the region $-5k_B T < \omega < 5k_B T$, which is relevant for transport. An analytical approach can be applied to the universal low-temperature regime of the two-channel Kondo model and we have shown that the saturation value of $\sim 0.388k_B/|e|$ can be computed numerically to high precision.

The very different spin-thermoelectric responses in the three classes of quantum impurity models discussed here could thus be used to experimentally discriminate over-screened and underscreened behaviour from the regular Fermi liquid behaviour with confidence. This is related to the different responses of the spectral function on the magnetic field found in these three cases. We speculate that all models with $S = n/2$ (full screening) are characterized by a spin Seebeck coefficient peak at $\sim T_K$ with decreasing height, all models with $S > n/2$ (underscreening) are characterized by a peak at $\sim B$ (perhaps with some logarithmic corrections) with decreasing height, while in models with $S < n/2$ (overscreening) the spin Seebeck coefficient peaks at the crossover scale and its height saturates. Here S is the impurity spin, while n is the number of screening channels.

On the applied side, the spin-thermoelectric effect might be of interest for spintronics as it enables generation of the spin current without any accompanying charge current. In this respect we note that the overscreened Kondo model outperforms the exactly screened and the underscreened ones, especially at magnetic fields below and around the Kondo temperature. The universal dependence of spin Seebeck coefficient on temperature with the peak position specified by magnetic field could be considered also for sensitive measurements of the magnetic field. It would be fascinating if the overscreened model that is playing such an important role in the fundamental studies of correlated electrons, ended up in a useful device.

Acknowledgments

We acknowledge the support of the Slovenian Research Agency (ARRS) under Program P1-0044.

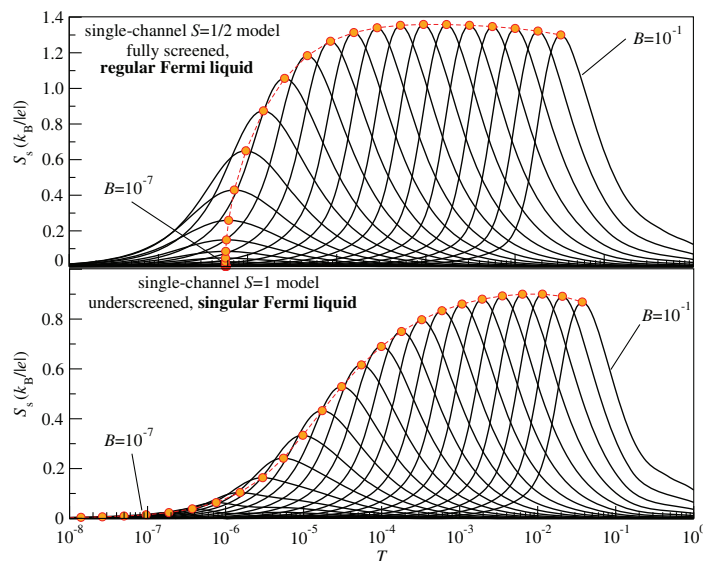


Figure A.1. Spin Seebeck coefficient for the single-channel Kondo model with $S = 1/2$ (top) and $S = 1$ (bottom). The magnetic field ranges from $B = 10^{-7}$ to 10^{-1} in steps of factor $10^{1/4}$.

Appendix. Spin Seebeck coefficient in single-channel problems

For reference and easier comparisons, in this appendix we provide the results for the spin Seebeck coefficient for the single-channel Kondo models (figure A.1). They are computed in exactly the same way and with exactly the same parameters as in figure 2. The positions of the maxima in the spin Seebeck coefficient are plotted in figure 3.

References

- [1] Hewson A C 1993 *The Kondo Problem to Heavy-Fermions* (Cambridge: Cambridge University Press)
- [2] Goldhaber-Gordon D, Shtrikman H, Mahalu D, Abusch-Magder D, Meirav U and Kastner M A 1998 Kondo effect in a single-electron transistor *Nature* **391** 156
- [3] Roch N, Florens S, Costi T A, Wernsdorfer W and Balestro F 2009 Observation of the underscreened Kondo effect in a molecular transistor *Phys. Rev. Lett.* **103** 197202
- [4] Yu L H and Natelson D 2004 The Kondo effect in C_{60} single-molecule transistors *Nanolett.* **4** 79
- [5] Nygard J, Cobden D H and Lindelof P E 2000 Kondo physics in carbon nanotubes *Nature* **408** 342
- [6] Kouwenhoven L and Glazman L 2001 Revival of the Kondo effect *Phys. World* **14** 33
- [7] Nozières P 1974 Fermi-liquid description of Kondo problem at low temperatures *J. Low. Temp. Phys.* **17** 31
- [8] Hewson A C, Oguri A and Meyer D 2004 Renormalized parameters for impurity models *Eur. Phys. J. B* **40** 177
- [9] Hewson A C 2005 The strong coupling fixed-point revisited *J. Phys. Soc. Japan* **74** 8
- [10] Mehta P, Andrei N, Coleman P, Borda L and Zaránd G 2005 Regular and singular Fermi-liquid fixed points in quantum impurity models *Phys. Rev. B* **72** 014430
- [11] Parks J J *et al* 2010 Mechanical control of spin states in spin-1 molecules and the underscreened Kondo effect *Science* **328** 1370
- [12] Logan D E, Wright C J and Galpin M R 2009 Correlated electron physics in two-level quantum dots: phase transitions, transport and experiment *Phys. Rev. B* **80** 125117

- [13] Žitko R, Mravlje J and Haule K 2012 Ground state of the parallel double quantum dot system *Phys. Rev. Lett.* **108** 066602
- [14] Cragg D M and Lloyd P 1979 Kondo Hamiltonians with a non-zero ground-state spins *J. Phys. C: Solid State Phys.* **12** L215
- [15] Sacramento P D and Schlottmann P 1989 Thermodynamics of the single-channel Kondo impurity of spin $s(\leq 7/2)$ in a magnetic field *Phys. Rev. B* **40** 431
- [16] Coleman P and Pepin C 2003 Singular Fermi liquid behavior in the underscreened Kondo model *Phys. Rev. B* **68** 220405
- [17] Koller W, Hewson A C and Meyer D 2005 Singular dynamics of underscreened magnetic impurity models *Phys. Rev. B* **72** 045117
- [18] Nozières P and Blandin A 1980 Kondo effect in real metals *J. Physique* **41** 193
- [19] Affleck I and Andreas Ludwig W W 1991 Critical theory of overscreened Kondo fixed points *Nucl. Phys. B* **360** 641
- [20] Affleck I 2005 Non-Fermi liquid behavior in Kondo models *J. Phys. Soc. Japan* **74** 59
- [21] Tóth A I and Zaránd G 2008 Dynamical correlations in the spin-half two-channel Kondo model *Phys. Rev. B* **78** 165130
- [22] Maldacena J M and Ludwig A W W 1997 Majorana fermions, exact mapping between quantum impurity fixed points with four bulk fermion species and solution of the unitarity puzzle *Nucl. Phys. B* **506** 565
- [23] Potok R M, Rau I G, Shtrikman H, Oreg Y and Goldhaber-Gordon D 2007 Observation of the two-channel Kondo effect *Nature* **446** 167
- [24] Costi T A and Zlatić V 2010 Thermoelectric transport through strongly correlated quantum dots *Phys. Rev. B* **81** 235127
- [25] Cornaglia P S, Usaj G and Balseiro C A 2012 Tunable charge and spin Seebeck effects in magnetic molecular junctions *Phys. Rev. B* **86** 041107
- [26] Rejec T, Žitko R, Mravlje J and Ramšak A 2012 Spin thermopower in interacting quantum dots *Phys. Rev. B* **85** 085117
- [27] Andergassen S, Costi T A and Zlatić V 2011 Mechanism for large thermoelectric power in molecular quantum dots described by the negative- u Anderson model *Phys. Rev. B* **84** 241107
- [28] Furuya K and Lowenstein J H 1982 Bethe-ansatz approach to the Kondo model with arbitrary impurity spin *Phys. Rev. B* **25** 5935
- [29] Andrei N and Destri C 1984 Solution of the multichannel Kondo problem *Phys. Rev. Lett.* **52** 364
- [30] Sacramento P D and Schlottmann P 1991 Thermodynamics of the n -channel Kondo model for general n and impurity spin S in a magnetic field *J. Phys.: Condens. Matter* **3** 9687
- [31] Zaránd G, Borda L, von Delft J and Andrei N 2004 Theory of inelastic scattering from magnetic impurities *Phys. Rev. Lett.* **93** 107204
- [32] Borda L, Fritz L, Andrei N and Zaránd G 2007 Theory of inelastic scattering from quantum impurities *Phys. Rev. B* **75** 235112
- [33] Wilson K G 1975 The renormalization group: critical phenomena and the Kondo problem *Rev. Mod. Phys.* **47** 773
- [34] Krishna-murthy H R, Wilkins J W and Wilson K G 1980 Renormalization-group approach to the Anderson model of dilute magnetic alloys: I. Static properties for the symmetric case *Phys. Rev. B* **21** 1003
- [35] Costi T A 2000 Kondo effect in a magnetic field and the magnetoresistivity of Kondo alloys *Phys. Rev. Lett.* **85** 1504
- [36] Rosch A, Costi T A, Paaske J and Wölfle P 2003 Spectral function of the Kondo model in high magnetic field *Phys. Rev. B* **68** 014430
- [37] Bulla R, Costi T and Pruschke T 2008 The numerical renormalization group method for quantum impurity systems *Rev. Mod. Phys.* **80** 395
- [38] Weichselbaum A and von Delft J 2007 Sum-rule conserving spectral functions from the numerical renormalization group *Phys. Rev. Lett.* **99** 076402

- [39] Nguyen T K T, Kiselev M N and Kravtsov V E 2010 Thermoelectric transport through a quantum dot: effects of the asymmetry in Kondo channels *Phys. Rev. B* **82** 113306
- [40] Mitchell A K and Sella E 2012 Universal low-temperature crossover in two-channel Kondo models *Phys. Rev. B* **85** 235127
- [41] Affleck I and Ludwig A W W 1993 Exact conformal-field-theory results on the multichannel Kondo effect: single-fermion Green's function, self-energy and resistivity *Phys. Rev. B* **48** 7297
- [42] Tóth A I, Borda L, von Delft J and Zaránd G 2007 Dynamical conductance in the two-channel Kondo regime of a double quantum dot *Phys. Rev. B* **76** 155318